

# Stability analysis and charts for slopes susceptible to translational failure

Hisham T. Eid, Azza M. Elleboudy, Hazem G. Elmarsafawi, and Amani G. Salama

**Abstract:** The aim of this paper is to develop two- and three-dimensional stability charts for slopes susceptible to translational failure. An extensive parametric study was conducted using a slope model that is designed to simulate field conditions with respect to configurations of the sliding mass, and unit weight and shear strength of the involved materials. Slopes subjected to different conditions of pore-water pressures and seismic forces were considered in the study. The study shows the special importance and difficulties of considering the end effects in the analysis of translational slope failures and suggests a method for quantifying and incorporating them. Charts presented in this paper do not require an iterative procedure in determining factor of safety. They give the practicing geotechnical engineer a fast and reliable method to estimate the two and three-dimensional factors of safety for slopes susceptible to translational mode of failure and to back-calculate the mobilized shear strength of materials involved in slope failures following such mode. Numerical examples are given to illustrate different uses of these charts.

*Key words:* slope stability analysis, translational failure, two-dimensional analysis, three-dimensional analysis, seismic forces.

**Résumé :** Le but de cet article est de développer des diagrammes de stabilité à deux et trois dimensions pour des talus susceptibles d'atteindre la rupture par translation. On a conduit une vaste étude paramétrique au moyen d'un modèle de talus qui est conçu pour simuler les conditions de terrain en fonction des configurations de la masse en mouvement, du poids volumique et de la résistance au cisaillement des matériaux impliqués. Dans cette étude, on a considéré des talus soumis à différentes conditions de pressions interstitielles et de forces sismiques. L'étude montre l'importance particulière et les difficultés de prendre en considération les effets des extrémités dans l'analyse des ruptures par translation et suggère une méthode pour les quantifier et les incorporer. Les diagrammes présentés dans cet article ne requièrent pas de procédure d'itération pour déterminer le coefficient de sécurité. Ils donnent à l'ingénieur praticien en géotechnique une méthode rapide et fiable d'estimer les coefficients de sécurité pour des pentes à deux et trois dimensions susceptibles au mode de rupture par translation et de calculer à rebours la résistance au cisaillement mobilisée des matériaux impliqués dans les ruptures de talus selon chaque mode. On donne des exemples numériques pour illustrer différentes utilisations de ces diagrammes.

*Mots clés :* analyse de stabilité des talus, rupture par translation, analyse bidimensionnelle, analyse tridimensionnelle, forces sismiques.

[Traduit par la Rédaction]

## Introduction

The generic terms, slope failures or landslides, embrace those down-slope movements of soil or rock masses that occur primarily as a result of shear failure at the boundaries of the moving mass. Slopes slide in two basic modes, rotational and translational. Unlike rotational slides, translational slides usually result from the presence of a heterogeneity located beneath the slope surface in the form of a strong material underlain by a weaker one. Such a situation creates a rela-

tively planar shear surface and predominantly translational slide movement.

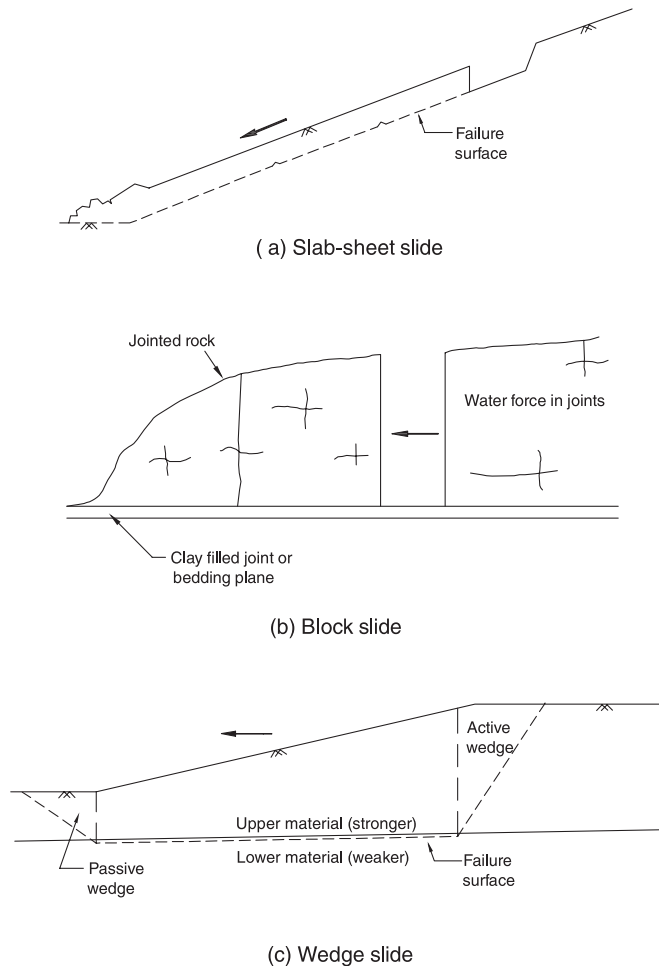
Figure 1 shows the three types of translational sliding modes for slopes, namely, slab-sheet, block, and wedge slide types. Slides of the slab-sheet type commonly occur in weathered colluvial material or residual soil associated with high water level having a sliding mass with depth to length ratio of less than 0.12 (Skempton 1953). Slides through composite cover systems of waste disposal facilities also belong to this category. Case histories of slab-sheet slides were described by several researchers (e.g., Vargas and Pichler 1957; Hutchinson 1967; Scranton 1996). Cases of block slides were also reported in the literature (e.g., McCallum 1930; Esu 1966; Elleboudy 1985). In these slides, the involved block separates from its jointed parent rock mass, usually sandstone or limestone, and slides as a unit on a well-defined plane of weakness formed by filled joint, bedding plane, or wet shale layer surface. Existence of water plays an important role by reducing shear strength along the block base and (or) exerting thrust forces in infiltrated joints. The third type of translational sliding mode is the wedge

Received 27 April 2005. Accepted 22 July 2006. Published on the NRC Research Press Web site at <http://cgj.nrc.ca> on 19 January 2007.

**H.T. Eid,<sup>1,2</sup> A.M. Elleboudy, H.G. Elmarsafawi, and A.G. Salama.** Banha University, Faculty of Engineering, Civil Engineering Department, Cairo 11629, Egypt.

<sup>1</sup>Corresponding author (e-mail: [heid@qu.edu.qa](mailto:heid@qu.edu.qa)).

<sup>2</sup>Present address: Qatar University, College of Engineering, Civil Engineering Department, Doha, Qatar, P.O. Box 2713, Doha, Qatar.

**Fig. 1.** Types of translational sliding modes for slopes.

slide. The name indicates the possibility of dividing the sliding mass into a middle wedge surrounded by active and passive wedges at the slope back and toe, respectively (Fig. 1c). This type is distinguished from the other two types by the significant contribution of shear strength of the upper (stronger) material in slope stability. Higher shear strength is mobilized along the back scarp and sides of the sliding mass compared to that mobilized along its base. Low shear strength at the base usually results from sliding through a preexisting failure surface along which residual shear strength is mobilized in soils (e.g., Gretton embankment failure (Chandler and Pachakis 1973); Maymont slide (Krahn et al. 1979); Gardiner Dam movement (Jaspar and Peters 1979); the Denholm landslide (Sauer and Christiansen 1987); Portuguese Bend slide (Ehlig 1992); Oceanside Manor slide (Stark and Eid 1992); Cincinnati landfill slide (Eid et al. 2000)). Low shear strength can also be mobilized along the geosynthetic interface of landfill liner systems (e.g., Kettleman Hills waste repository slide (Seed et al. 1990; Byrne et al. 1992)).

Slides of the wedge type occur more frequently and need lengthy analysis compared to the other two translational slide types that can be analyzed using the simple infinite slope stability concept. The end effects are usually ignored in the analysis of slab-sheet and block slides because of the shallow depth of sliding mass and the possible joint exist-

tence at sides of the sliding blocks, respectively. As a result, the study presented in this paper focuses on developing two-dimensional (2D) and three-dimensional (3D) stability charts for slopes susceptible to the wedge type of translational failure through conducting an extensive parametric study. In addition, the general name of the failure mode “translational” is used to refer to this type throughout the rest of this paper.

## Existing stability charts

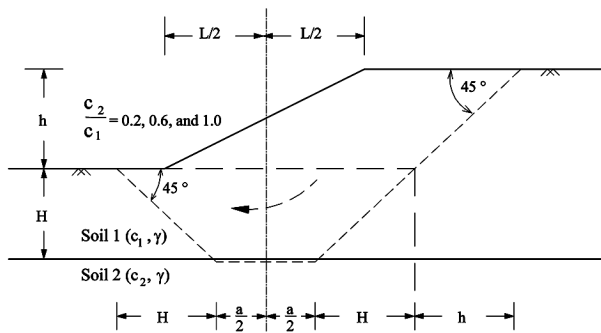
Stability charts for slopes susceptible to translational failures or failures along bilinear and trilinear slip surfaces are limited in the literature compared to those dealing with the rotational mode of failure such as the 2D stability charts presented by Taylor (1937), Bishop and Morgenstern (1960), Bell (1966), O’Connor and Mitchell (1977), Cousins (1978), and Michalowski (2002) and the 3D stability ones presented by Baligh and Azzouz (1975), Leshchinsky and Baker (1986), Gens et al. (1988), and Madej and Gajewski (1988). In addition, the use of the available charts for translational mode is restricted because they are developed for narrow ranges of material properties and sliding mass configurations.

Montés et al. (1996) presented charts to determine both the minimum 2D factor of safety ( $F_{2D}$ ) and the corresponding trilinear slip surface of slopes in cohesive soils. For the particular condition of short-term stability (i.e.,  $\phi = 0$  condition), an explicit formula was presented to calculate the factor of safety. Simplified Janbu approach (Janbu et al. 1956) was used in developing charts for cases of homogenous and stratified soil, with each layer having its own distinct undrained shear strength. The 2D slope model that was utilized by Montés et al. (1996), and reformed to the special case profile similar to that shown in Fig. 1c with cohesion of upper and lower soils of  $c_1$  and  $c_2$ , respectively, is shown in Fig. 2a. It can be seen that the proposed critical slip surface has a base centered on the vertical axis at midslope and inclined sides making an angle of  $45^\circ$  with respect to the horizontal. Stability charts for cases of cohesion ratio, i.e.,  $c_2/c_1$ , of 0.2, 0.6, and 1.0 were presented.

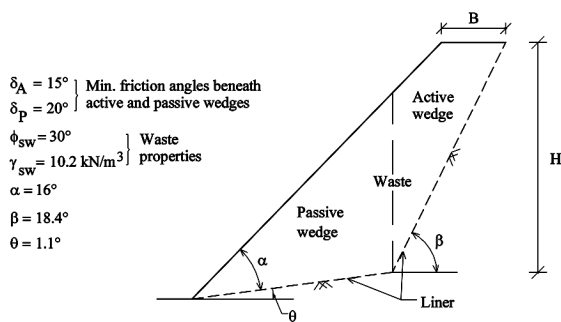
Qian et al. (2003) presented charts to calculate  $F_{2D}$  against translation failure for waste landfill slopes. The 2D slope model and material properties utilized in the analysis are shown in Fig. 2b. A two-part wedge analysis was developed and used to calculate  $F_{2D}$  for the slope model or the proposed waste–liner configuration. Existence of pore-water pressure was not considered in the analysis. The cohesion ( $c'$ ) of the waste and the interface adhesion of the liner component surfaces—if any—were omitted in this analysis due to the uncertainty in the values of these parameters. Furthermore, ignoring them simplified the analysis and led to conservative calculated factor of safety.

Lovell (1984) presented a chart for determining the 3D factor of safety ( $F_{3D}$ ) against translational slope failure. The chart was developed based on software that utilizes a method of columns as an extension to the method of slices in 2D analysis. The 3D slope model and material properties used in the analysis and the corresponding developed charts are shown in Fig. 2c. It can be seen that the shear strength of the lower (weaker) layer was assigned a constant value ( $c' = 9.6$  kPa) while that of the upper (stronger) layer was ex-

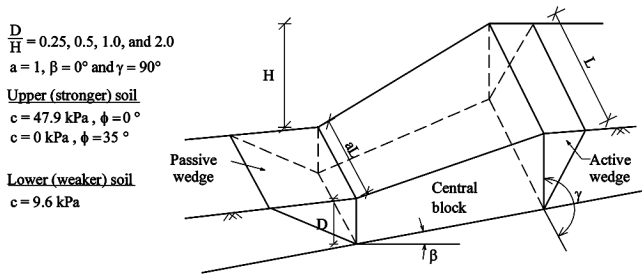
**Fig. 2.** Slope models and material properties utilized to develop existing stability charts.



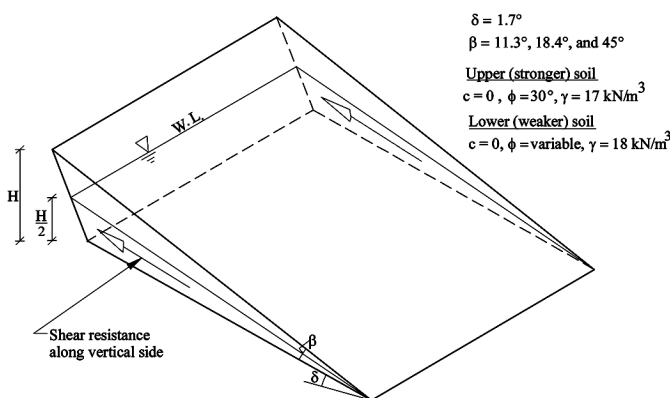
(a) Slope of cohesive soils (modified from Montés et al. 1996)



(b) Lined waste slope (modified from Qian et al. 2003)



(c) Three-block model (modified from Lovell 1984)



(d) Model with uniform cross sections (modified from Arellano and Stark 2000)

pressed in two alternatives only. Groundwater was not included in the analysis. In addition, the sides of the sliding mass were taken to be vertical.

Stark and Eid (1998) showed that commercially available 3D slope stability software has an inherent limitation that leads to underestimation of  $F_{3D}$  for a translational failure mode. The software divides the sliding mass into vertical columns. The resisting forces are calculated by considering only the material shear strength along the base of each column. As a result, the shear resistance due to cohesion and (or) friction generated by the earth pressure on vertical sides of the sliding mass is ignored. In translational failures, vertical sides provide the minimum amount of shear resistance because the effective normal stress acting on these sides is only due to the lateral earth pressure and a vertical side produces the minimum area of shear surface. As a result, case histories of translational failure usually exhibit vertical sides to significant underestimation of the  $F_{3D}$  in case of translational failures. In addition, it results in overestimation of the back-calculated shear strength of the materials involved in a slope failure. Using a cumbersome technique to overcome this limitation and considering shear resistance due to mobilization of the at-rest earth pressure on the two parallel vertical sides of the sliding mass, Stark and Eid (1998) showed that this overestimation in 3D back-calculated friction angles for a translational failed slope can be as large as 30%.

In a further study of the importance of 3D slope stability analyses in practice, Arellano and Stark (2000) used a more direct technique to overcome the software limitation by applying an external force equivalent to the shear resistance due to the at-rest earth pressure acting at the centroid of each of the two vertical sides of a slope model. Figure 2d shows this model and the material properties utilized in the study. One value for each of the unit weight and the friction angle for the upper material and the unit weight and the surface inclination angle of the lower material was utilized in the study. It should be noted that the slope model is simplified to comprise a sliding surface passing through the crest and toe of the slope and a water table located at the head scarp and exhibits a uniform cross section across the slope that yields the same  $F_{2D}$ . Consequently, the  $F_{3D}$  obtained from an analysis performed without considering the shearing resistance along the vertical sides of the sliding mass is similar to that corresponding to 2D analysis.

### Method of analysis

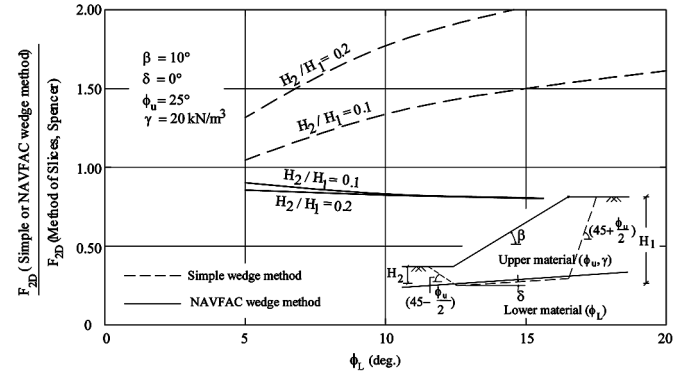
As previously mentioned, a translational sliding mass can be divided into three wedges separated by vertical boundaries. The middle wedge is surrounded at the crest and toe of the slope by two wedges assumed to be in active and passive states, respectively. Based on Rankine's theory and having  $\phi_U$  representing the friction angle of the upper material, two shear planes inclined at angles of  $45 + \phi_U/2$  and  $45 - \phi_U/2$  with the horizontal can be drawn reflecting these two stress conditions, respectively. Because of this wedged nature, two methods of wedge analysis are usually considered, in addi-

tion to the method of slices, in limit equilibrium analysis of translational failure. The first one is the simple wedge method (Lambe and Whitman 1969) in which the stability of the middle wedge is considered in calculating  $F_{2D}$  while representing the effect of the surrounding wedges simply by the active and passive earth pressure forces. The second one is the wedge method proposed in NAVFAC (1971) in which shear strengths along the slip surfaces of the active and passive wedges are considered, in addition to the earth pressure forces, in the stability of the middle wedge. For the proposed slope conditions, Fig. 3 shows factors of safety calculated using these two wedge methods compared to those calculated using method of slices and employing Spencer's stability procedure (Spencer 1967). Spencer's method assumes that the resultant interslice forces have the same inclination throughout the sliding mass. Both force and moment equilibriums are satisfied in Spencer's method. This method is regarded as being accurate, i.e., within 6% of the correct 2D factor of safety (Duncan 1992). This statement is especially true for the translational failure mode in which the inclination of the interslice forces within the major part of the slope is nearly constant.

It can be seen from Fig. 3 that the simple wedge method overestimates the calculated  $F_{2D}$  while the NAVFAC (1971) wedge method underestimates it. The error magnitude is enhanced for higher values of  $H_2/H_1$ , where  $H_1$  and  $H_2$  are defined as the vertical distances from the point at which surface of the weaker material passes beneath the crest and toe of the slope, respectively. The error is significant even in case of low values of weaker material friction angle ( $\phi_L$ ) that usually causes translational failures. As a result, neither of these two methods was used in the current parametric study in spite of their simplicity in 2D stability analysis. Spencer's method of slices utilized in the slope stability computer program UTEXAS3 (Wright 1992) was employed in all of the 2D stability analyses conducted to develop the 2D stability charts presented in this study.

The available 3D slope stability software do not utilize a 3D extension of Spencer's method. They utilize the extensions of Bishop's and Janbu's methods of slices (Bishop 1955; Janbu et al. 1956). Bishop's simplified method was originally derived for a rotational failure mode. It neglects vertical interslice forces and calculates the factor of safety based on moment equilibrium, while horizontal force equilibrium is neglected. Janbu's simplified method assumes that the resultant interslice forces are horizontal. The factor of safety is calculated based on force equilibrium, while moment equilibrium is not satisfied. As a result, Janbu's simplified method was utilized in 3D stability analysis conducted in this study because it is more suitable for a translational failure mode. Because it is user friendly and has more capability in describing external loads and performing 2D analysis out of 3D data file, the slope stability program CLARA 2.31 (Hungry 1988) was used for the 3D stability analyses described in the present paper. The program utilizes an extension of Bishop's and Janbu's simplified methods of slices. The CLARA 2.31 program was not used in 2D stability analysis except in the case of comparing  $F_{3D}$  to  $F_{2D}$ . In this case, both of the safety factors were determined using the same program (CLARA 2.31) and method of slices (Janbu's

**Fig. 3.** Two-dimensional factors of safety determined using simple wedge and NAVFAC (1971) wedge methods. These are compared to the factors of safety determined using the method of slices.



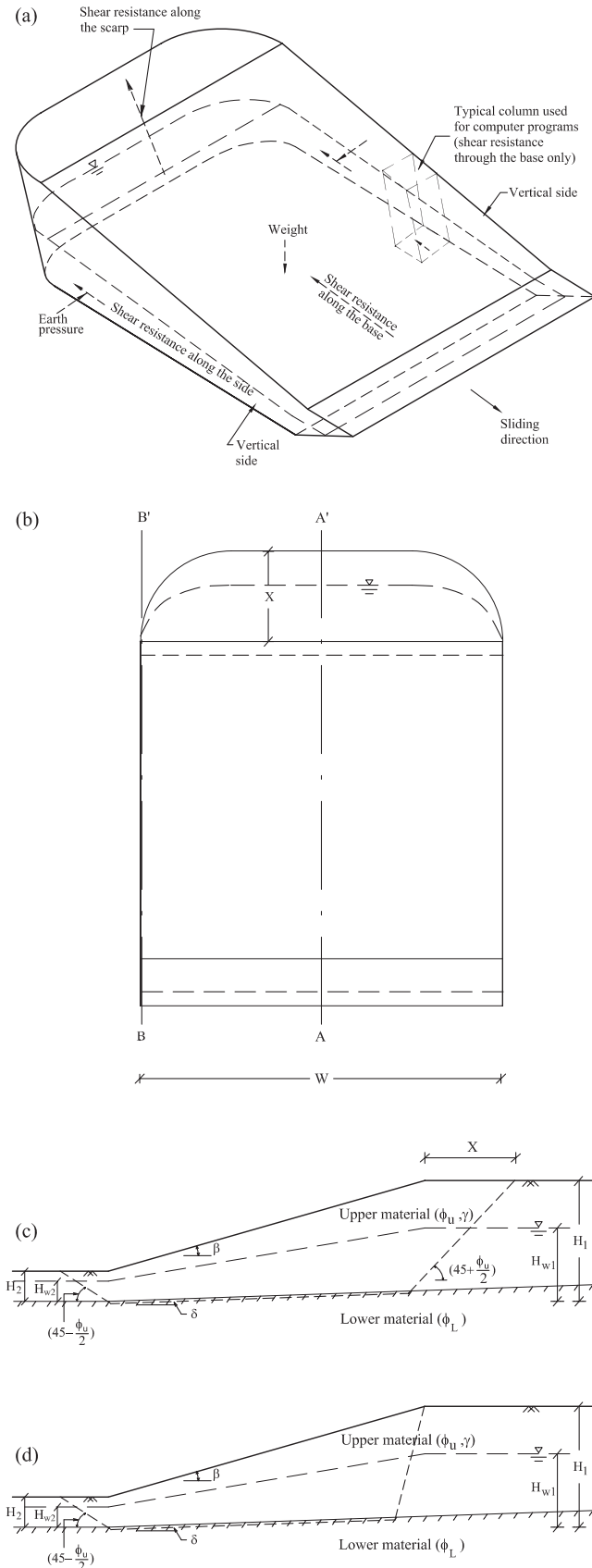
simplified method) to have compatible values. It should be noted also that the calculated  $F_{3D}$  and the corresponding  $F_{2D}$  that were determined using the same method were dealt with throughout the analysis and charts presented in this paper as a ratio ( $F_{3D}/F_{2D}$ ). This assures data consistency even when using the 2D stability charts—developed utilizing Spencer's method—in conjunction with the 3D stability charts (i.e.,  $F_{3D}/F_{2D}$  charts)—developed utilizing Janbu's simplified method—for the analysis of the same slope.

### Design of slope model for parametric study

A slope model was designed and employed to conduct the parametric study needed for the development of 2D and 3D stability charts. A number of field case histories that experienced translational failure were studied to design the slope model so that it simulates field conditions with respect to sliding mass configurations, pore-water pressures, and material properties. Figures 4a, 4b, 4c, and 4d show a 3D view, plan, critical cross section, and near side cross section of this model, respectively. The model represents a sliding mass, with similar critical cross sections (Fig. 4c), that is rounded at the ends of its back scarp creating a group of noncritical near side cross sections and bounded by two vertical sides at a distance  $W$  (slope width). Case histories in which curved surfaces that connect the inclined back scarp to the two vertical sides of sliding mass have been reported by several researchers (e.g., Bromhead 1986; Stark and Eid 1998).

It can be seen that this model is distinguished from those used in previous studies in several aspects that make it more representative of field case histories and more generic. For the 3D condition, the model incorporates vertical sides and rounded ends of back scarps. For both 2D and 3D conditions, it considers the possibility of locating the weak material at a depth  $H_2$  below the slope toe and having a top width for the sliding mass. As will be shown subsequently, this width depends on the slope geometry and material properties that lead to a back scarp the bottom of which is not necessarily an orthogonal projection of the slope crest line. These conditions were frequently reported for translational slope failures (e.g., Skempton and Petley 1967; Chandler et al. 1973; Cruden et al. 1991) but not represented by one model

**Fig. 4.** Slope model used in the analysis: (a) 3D view; (b) plan view; (c) section A–A' representing critical cross sections; (d) section B–B' representing the vertical sides of the model.



in the literature. The sliding surface is taken to consist of a back scarp that is inclined at  $45 + \phi_U/2$  with the horizontal, connected to the bottom part that extends 0.1 m into the lower material and runs parallel to its surface until it rises at  $45 - \phi_U/2$  starting from a point directly below the toe to daylight (Figs. 4c and 4d). Values of 0, 0.25, and 0.50 are assigned for  $H_2/H_1$  in this study. Slope angle ( $\beta$ ) is taken to be either  $10^\circ$ ,  $20^\circ$ , or  $30^\circ$ . The weaker material surface is assumed to have an inclination ( $\delta$ ) of  $0^\circ$ ,  $3^\circ$ , and  $6^\circ$  to simulate natural bedding planes, commonly encountered preexisting slip surfaces, or the nearly horizontal part of landfill liner systems.

Reported case histories showed that translational failure often involves a drained shearing condition, i.e., long-term failure condition. Sliding in which drained residual shear strength is mobilized along a preexisting shear surface overlying stiff fissured clay that mobilizes drained fully softened shear strength is a typical translational failure case (Eid 1996). For this reason, shear strength of the upper (stronger) and lower (weaker) materials of the slope model were expressed only in terms of friction angles  $\phi_U$  and  $\phi_L$ , respectively, considering a linear drained shear strength envelope that passes through the origin. In case of nonlinear drained failure envelopes,  $\phi_U$  and  $\phi_L$  can represent the secant friction angles of linear envelopes formed by connecting the origin and the shear strengths at the average effective normal stresses acting on the failure surface portions slipping through the upper and lower materials, respectively.

Ranges of values for  $\phi_U$  and  $\phi_L$  utilized in the analysis are taken to be consistent with those reported for fully softened and residual friction angles, respectively. Consequently, values of friction angles higher than  $35^\circ$  were not considered because they exceed the upper limit of both the drained fully softened and residual friction angles reported for natural soils at ranges of average effective normal stress usually encountered in slope failure case histories (Skempton 1985; Mesri and Cepeda-Diaz 1986; Mesri and Abdel-Ghaffar 1993; Stark and Eid 1994, 1997). In addition, the minimum value assigned for  $\phi_L$  was  $4^\circ$ . Unit weights of the upper and lower materials ( $\gamma$ ) are assumed to be the same and equal to 14, 17, or 20 kN/m<sup>3</sup>. The low value of unit weight is included in the parametric study to cover cases of waste landfill slopes. It should be noted that failure of such slopes can involve shearing either along the soil–waste interface, liner components interfaces, or through the waste material, the shear strengths of which are mostly covered by the friction angle range considered in this study (Stark and Peoppel 1994; Kavazanjian et al. 1995; and Eid et al. 2000, respectively).

**Pore-water pressure representation**

Two methods were considered for representation of the pore-water pressures in the slope model used in the parametric study. The first method introduces water table elevations or piezometric surfaces; and the second method uses the pore-water pressure ratio ( $r_u$ ) as described by Bishop and Morgenstern (1960). Pore-water pressure ratio at a point is defined as the magnitude of pore-water pressure divided by the total stress at this point. Using  $r_u$  is a crude manner of accounting for the presence of water in a slope. Barnes (1999) showed that using a single  $r_u$  value to represent the

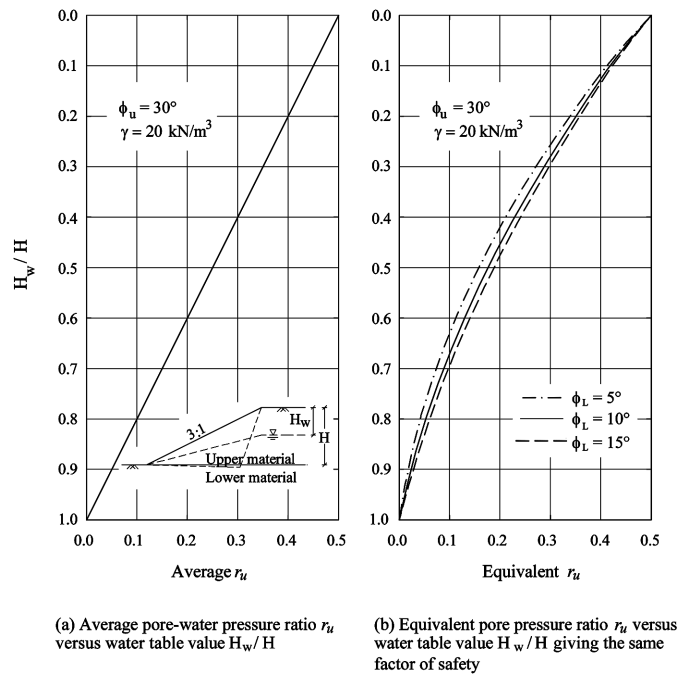
global pore-water pressure condition may lead to significant errors in slope stability analysis of circular failures. The error magnitude depends on the slope angle, the cohesion of soil and, to a lesser extent, the friction angle value. The technique used by Barnes (1999) was adopted in this study to figure out if the same conclusion could be drawn for the translational failure mode. For an example slope of inclination 3H:1V, values of the ratio of water height ( $H_w$ ) to the slope height ( $H$ ) were plotted against the corresponding values of both the average  $r_u$  proposed by Bishop and Morgenstern (1960), and equivalent  $r_u$  that gives the same factor of safety. The results are shown in Figs. 5a and 5b, respectively. Comparing the results of the two figures shows that, except for values of  $H_w/H$  equal to 0 and 1.0, using one average value for  $r_u$  overestimates the pore-water pressures. This overestimation increases with a decrease in  $\phi_L$ . The study also showed that this overestimation is not sensitive to values of  $\phi_U$  or  $\beta$ . To avoid this error and its consequences in stability analyses, pore-water pressures were represented in the slope model used in the present parametric study by introducing water table elevations. Groundwater tables having linearly decreasing heights and maintaining constant value of  $H_w/H$  (i.e., equal values of  $H_{w1}/H_1$  and  $H_{w2}/H_2$ ) are used for the slope model. Variables  $H_{w1}$  and  $H_{w2}$  are defined as the water heights near the slope crest and toe, respectively. Values for  $H_w/H$  of 0, 0.4, and 0.8 were utilized in the analyses.

### Top width of critical sliding mass

As shown in Fig. 4, the location at which the critical slip surface daylighted behind the slope crest, i.e., top width of critical sliding mass ( $X$ ), should be determined to define the configuration of the slope model. A supplementary 2D parametric study was conducted to develop a chart to determine  $X$  values leading to the minimum factor of safety based on material properties and slope geometry parameters. A searching technique was used to quantify the effect of these properties and parameters on the location of the critical slip surface. An example of the search procedure used for locating the critical slip surface is shown in Fig. 6a. The study revealed that  $X$  is insensitive to values of  $\phi_U$  and  $\delta$ . On the other hand, it increases with increasing values of  $\beta$  and  $H_2/H_1$ , and decreasing values of  $\phi_L$  (Fig. 6b). It can be noted also that, for the proposed configurations and shear strength conditions, the commonly used simple bilinear critical sliding surface that passes through the slope crest and toe can only be developed if the lower soil passes through the slope toe, i.e.,  $H_2 = 0$ . Development of  $X$  is directly proportional to the value of  $H_2$  because a larger driving force is needed to be built up by shifting the back scarp a distance behind the slope crest to counter the enhanced passive resisting forces created by increasing  $H_2$ .

Cracking that appears on slope top and delineates the extent of sliding mass behind the crest, i.e., value of  $X$ , is usually the first failure sign. This is supported by observations reported in the literature describing translational failure case histories (e.g., Stark et al. 2000). This may interpret the insensitivity of  $X$  to the value of  $\phi_U$ , which mainly controls the back-scarp inclination when the failure progresses down through the upper layer (Figs. 4c and 6b).

**Fig. 5.** Average and equivalent pore-water pressure ratios for 3H:1V slope.



(a) Average pore-water pressure ratio  $r_u$  versus water table value  $H_w/H$   
(b) Equivalent pore pressure ratio  $r_u$  versus water table value  $H_w/H$  giving the same factor of safety

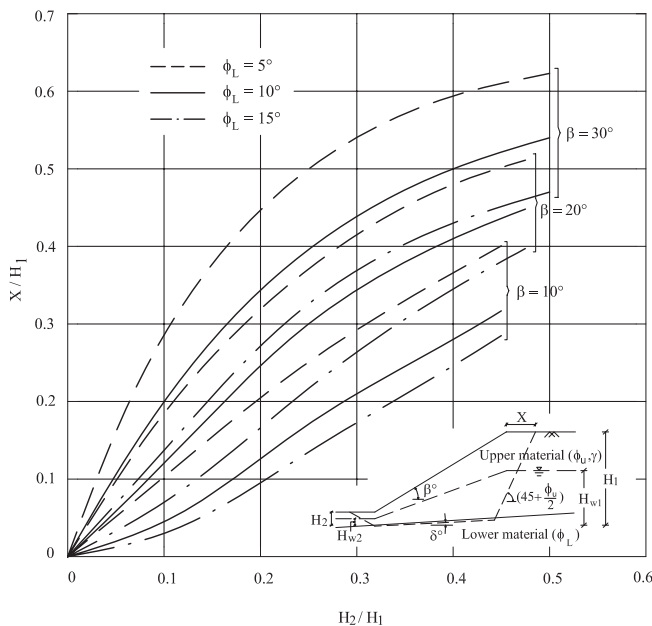
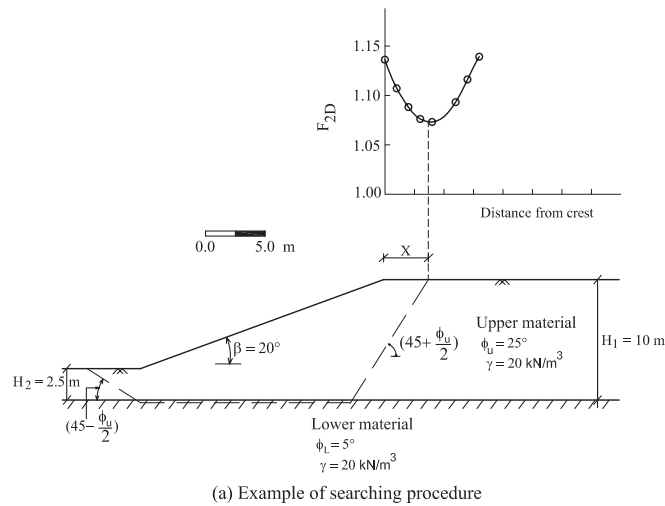
The relationship shown in Fig. 6b is recommended for locating the critical slip surface for simple slopes as a necessary step to estimate the minimum factor of safety against translational failure. In addition, it provides the slip surface location that is needed as an initial input to start a more sophisticated automatic search for locating the critical slip surface of complicated slopes susceptible to translational failure.

### Two-dimensional stability charts

Most slope stability analyses are performed using 2D limit equilibrium analysis because of its relative simplicity compared to 3D analysis. In addition, 2D analysis yields a conservative estimate for the factor of safety because the end effects are not included. While the use of software has superseded most graphical methods, charts for 2D slope stability analysis are still routinely used in practice. The charts presented in this section were developed to help in such purpose for the translational mode of failure. The parametric study used to develop the charts was conducted utilizing the 2D critical cross section of the slope model shown in Fig. 4c. To calculate the minimum factor of safety for this cross section, values of parameters  $H_1$ ,  $H_2$ ,  $\beta$ ,  $\delta$ ,  $\phi_L$ , and  $\gamma$  were first assumed. Using the chosen parameters, the value of top width of the critical sliding mass was determined and the corresponding  $F_{2D}$  was then calculated. This procedure was repeated using a variety of slope parameters.

Slopes with  $\beta < 10^\circ$  were not considered because they rarely experience stability problems. In addition, slopes with  $\beta$  that are equal to, or higher than, the maximum utilized value of  $\phi_U$ , i.e.,  $35^\circ$ , were not analyzed because the infinite slope failure mode rather than the translational mode would govern  $F_{2D}$  in such a condition. The same concept was also

Fig. 6. Top width of critical sliding mass ( $X$ ).



followed in developing the 3D stability charts presented in the subsequent section.

The analysis revealed that  $F_{2D}$  depends on the ratio of  $H_2$  to  $H_1$  rather than on their absolute values. As a result, the 2D stability charts developed in this study are grouped for cases of  $H_2/H_1$  of 0, 0.25, and 0.50 as presented in Figs. 7, 8, and 9, respectively. The same scale was used in all of the charts for easy comparison of the effect of different parameters. It should be noted that  $F_{2D}$  in these charts is presented as a function of the ratio of  $\tan \phi_L$  to  $\tan \phi_U$ . Consequently, determining  $F_{2D}$  does not require any iterative procedure because this ratio is independent of the safety factor that is equal for both  $\phi_L$  and  $\phi_U$ . This concept of utilizing a parameter in which the nominator and denominator include the safety factor in such a way that leads to its cancellation from both of them was first introduced by Bell (1966) for developing

charts for rotational failure of slopes in which the safety factor is applied to both  $c'$  and  $\tan \phi'$ .

The charts of Figs. 7, 8, and 9 show that  $F_{2D}$  increases with increasing values of  $H_2/H_1$ ,  $\phi_L$ , and  $\gamma$ , and decreasing values of  $H_w$ ,  $\beta$ , and  $\delta$ . They also show that the effect of flattening the slope to increase the factor of safety decreases in cases of low  $\phi_L$  to  $\phi_U$  ratio. This is indicated by the converging nature of  $F_{2D}$  at low values of  $\tan \phi_L / \tan \phi_U$ . Results also show that  $F_{2D}$  increases with increasing value of  $\phi_U$ . The influence of changing  $\gamma$  (within the utilized range) on  $F_{2D}$  values decreases with increasing  $\beta$  and  $\delta$ , and decreasing  $H_w$  values. For dry slopes, i.e.,  $H_w/H = 0$ , this effect is not significant and consequently not shown on charts (Charts a, b, and c in Figs. 7, 8, and 9). This may be attributed to the balanced effect of changing  $\gamma$ , i.e., changing the sliding mass weight, on both the driving and the resisting forces mobilized along the shear surface in such a way that  $F_{2D}$  remains almost the same. Having a high water table mainly reduces the weight imposed on the nearly horizontal part of the sliding surface on which the major part of the resisting forces against translational failure is mobilized. This reduction in weight and the associated decrease in resisting forces caused by having a submerged part of the sliding mass is more significant in case of low unit weights. As a result,  $F_{2D}$  against translational failure decreases with the decrease in unit weight of the sliding materials that are partly or wholly submerged below the water table. Due to differences in failure mode and mechanism, this conclusion is contrary to that reported by several researchers (e.g., Taylor 1937; Singh 1970; Michalowski 2002) for the effect of decreasing  $\gamma$  on  $F_{2D}$  against rotational failure for all of the pore-water pressure conditions.

### Three-dimensional stability charts

The 2D limit equilibrium methods calculate the factor of safety against failure for a slope assuming a plane-strain condition that ignores the shear resistance along the sides of the sliding mass. Slopes failing in a translational mode exhibit the most pronounced difference between  $F_{2D}$  and  $F_{3D}$  because of the large difference between the mobilized shear strength along the back scarp and sides of the sliding mass and that along the base. In addition, a translational failure can occur in relatively flat slopes because of the low shear strength of the underlying material. Chen and Chameau (1983) and Leshchinsky et al. (1985) showed that the flatter the slope, the greater the difference between  $F_{2D}$  and  $F_{3D}$ . As a result, ignoring this additional resistance may lead to overdesigned slopes and (or) overestimation of back-calculated shear strength parameters of materials involved in slopes that failed in a translational mode. The back-calculated parameters can be used in remedial measures for failed slopes or for slope design at sites with similar conditions.

Using the slope model shown in Fig. 4, a parametric study was conducted to develop charts relating the ratio  $F_{3D}/F_{2D}$  to slope geometry parameters and involved material properties. The value of  $F_{2D}$  used in these charts is that corresponding to the most critical cross section, i.e., the cross-section with the minimum  $F_{2D}$ , which is shown in Fig. 4c. Charts are pre-

Fig. 7. Two-dimensional stability charts for translational mode of failure for slopes with  $H_2/H_1 = 0.0$ .

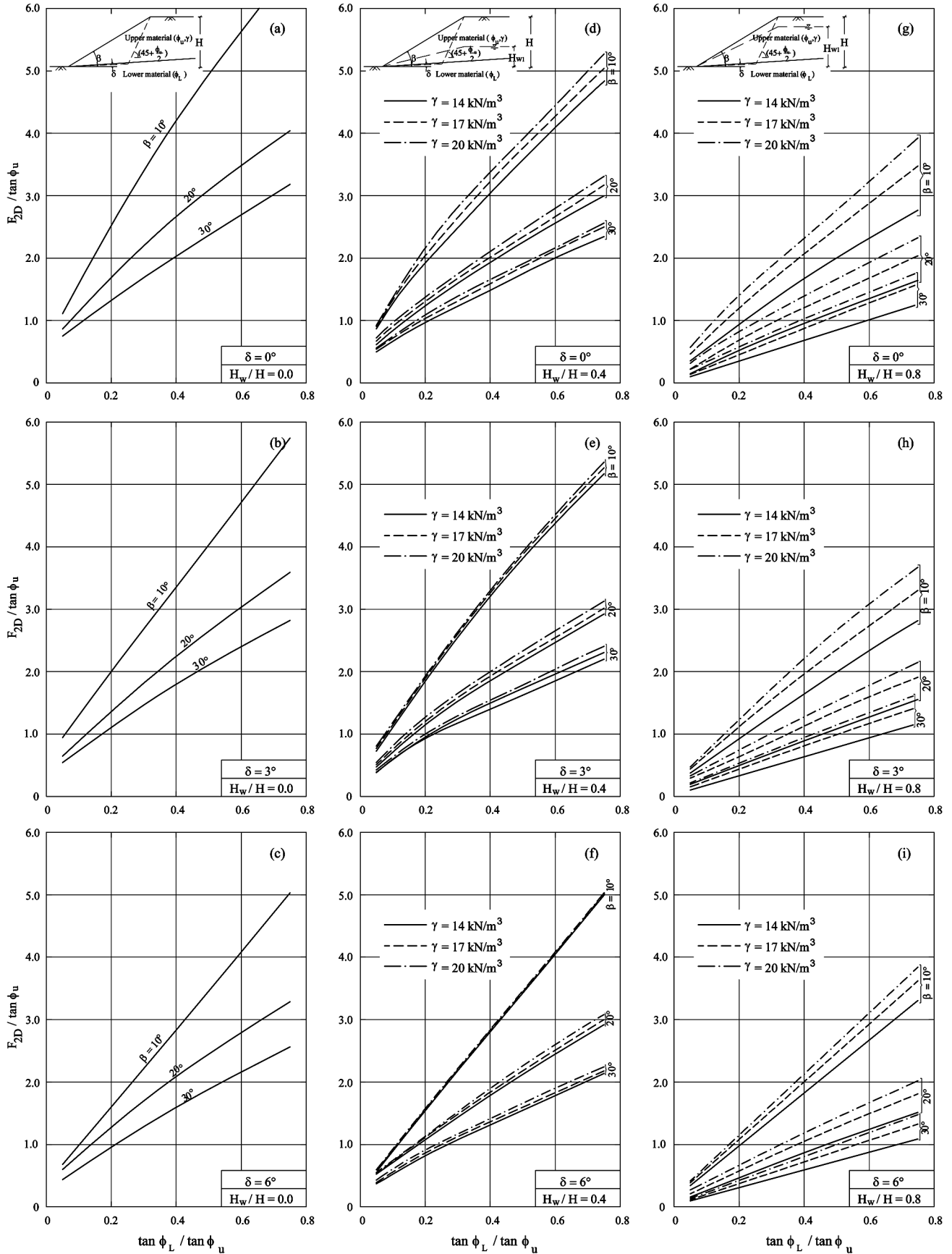


Fig. 8. Two-dimensional stability charts for translational mode of failure for slopes with  $H_2/H_1 = 0.25$ .

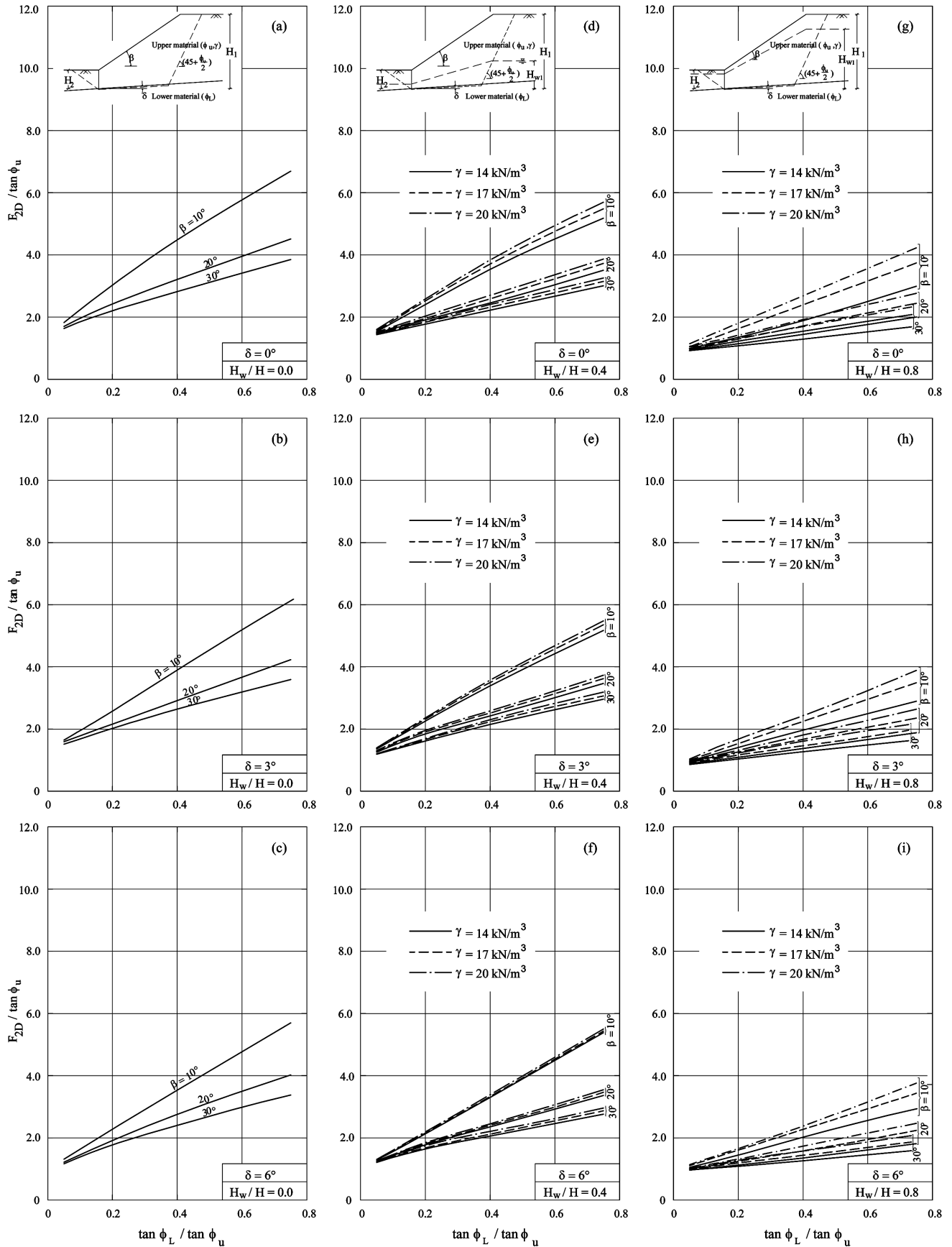
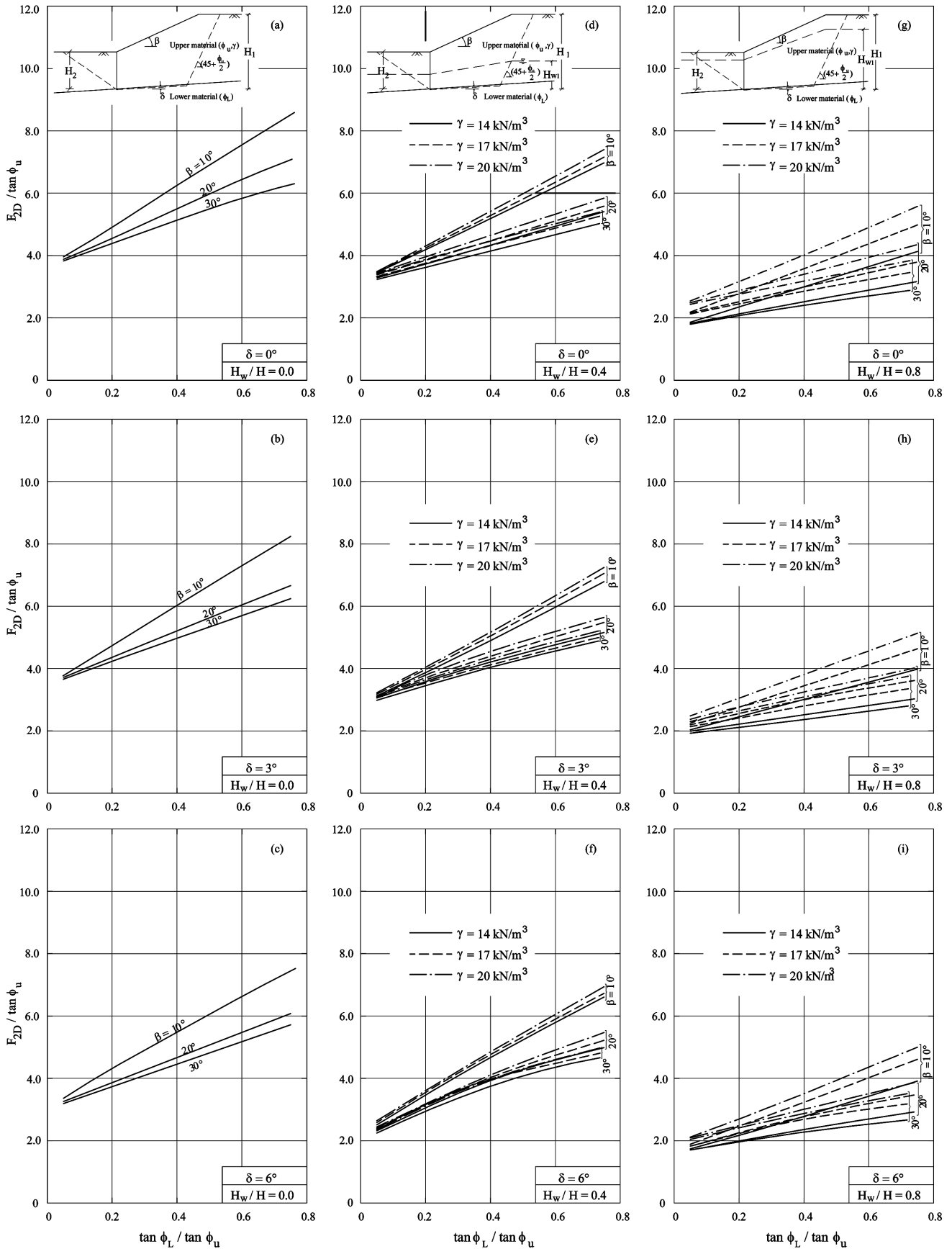


Fig. 9. Two-dimensional stability charts for translational mode of failure for slopes with  $H_2/H_1 = 0.5$ .



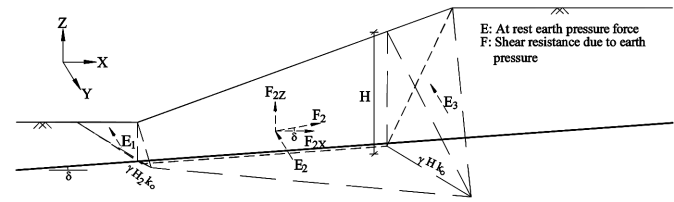
sented also for slopes exposed to seismic forces. The CLARA 2.31 slope stability program was used in these analyses. Geometry data is input into the CLARA 2.31 program through describing a series of 2D cross sections. The geometrical configurations of the 3D model shown in Fig. 4 were described using two sections similar to the critical one shown in Fig. 4c representing the middle part of the mass, two sections similar to that shown in Fig. 4d representing the vertical sides of the mass, and ten sections representing the two rounded parts of the back scarp.

As with all of the commercially available 3D slope stability analysis programs, the CLARA 2.31 program has an inherent limitation that ignores the shear resistance along the sliding mass vertical sides. To overcome this limitation, shear resistance along the two sides was included by imposing a group of external horizontal and vertical forces ( $F_x$  and  $F_z$ ) that are the components of the shear resistance forces ( $F$ ). Each shear resistance force was calculated by multiplying the corresponding earth pressure force ( $E$ ) acting perpendicular to the vertical sides by the tangent of  $\phi_U$ . Each earth pressure force was estimated as the volume of the at-rest earth pressure diagram imposed on the corresponding part of the slope vertical side. The coefficient of earth pressure at rest is taken as  $K_o = 1 - \sin \phi_U$ . Since the predominant movement direction in translational failures is parallel to the surface of the lower material, the shear resistance forces were assigned such direction (Fig. 10a). To be imposed on the opposite direction, forces generated by pore-water pressures were calculated using the same concept utilized for the shear resistance forces (Fig. 10b). It should be noted that all of the horizontal and vertical force components were imposed at the centroids of their corresponding areas of the vertical sides of sliding mass. This technique in quantifying and incorporating the end effects is different from that utilized by Arellano and Stark (2000) in which the earth pressure forces were approximated using the average vertical effective stress over the depth of the sliding mass.

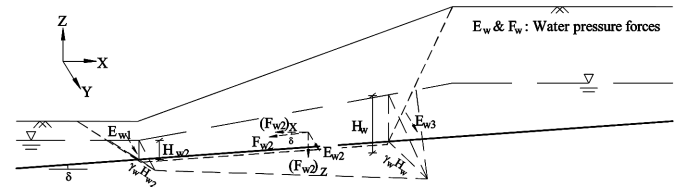
Figs. 11a, 11b, and 11c show the effect of sliding mass geometry and material properties on the ratio  $F_{3D}/F_{2D}$  for the slope model with  $H_2/H_1$  equal to 0.0, 0.25, and 0.5, respectively. The parametric study showed that  $F_{3D}/F_{2D}$  is not sensitive to the value of  $\phi_L$ . This conclusion agrees with data presented by Arellano and Stark (2000) showing a slight increase of the 3D effect with increasing  $\phi_U/\phi_L$  ratio using a constant  $\phi_U = 30^\circ$ . This can be interpreted in terms of the overwhelming effect of  $\phi_U$  over that of  $\phi_L$  on the value of  $F_{3D}$ , which mainly increases because of the inclusion of the shear resistance along the parallel vertical sides of sliding mass. The magnitude of such resistance is directly proportional to the value of  $\phi_U$ .

The present study also showed that  $\delta$ ,  $\gamma$ , and  $H_w$  have a slight effect on  $F_{3D}/F_{2D}$  values. As a result, these parameters were not included in the 3D stability charts. It can be seen that for the same sliding mass  $F_{3D}$  is greater than  $F_{2D}$  of its critical cross section regardless of slope geometry configurations and values of the material properties. The 3D effect, i.e., the  $F_{3D}/F_{2D}$  value decreases with increasing  $W/H_1$  ratios for a given slope due to the domination of the increasing weight of sliding mass and its corresponding driving forces over the constant shear resistance along the parallel vertical sides. Figure 11 also shows that for slopes with the same

**Fig. 10.** Forces imposed on the vertical sides of slope model in the stability analysis.



(a) Forces generated by earth pressure



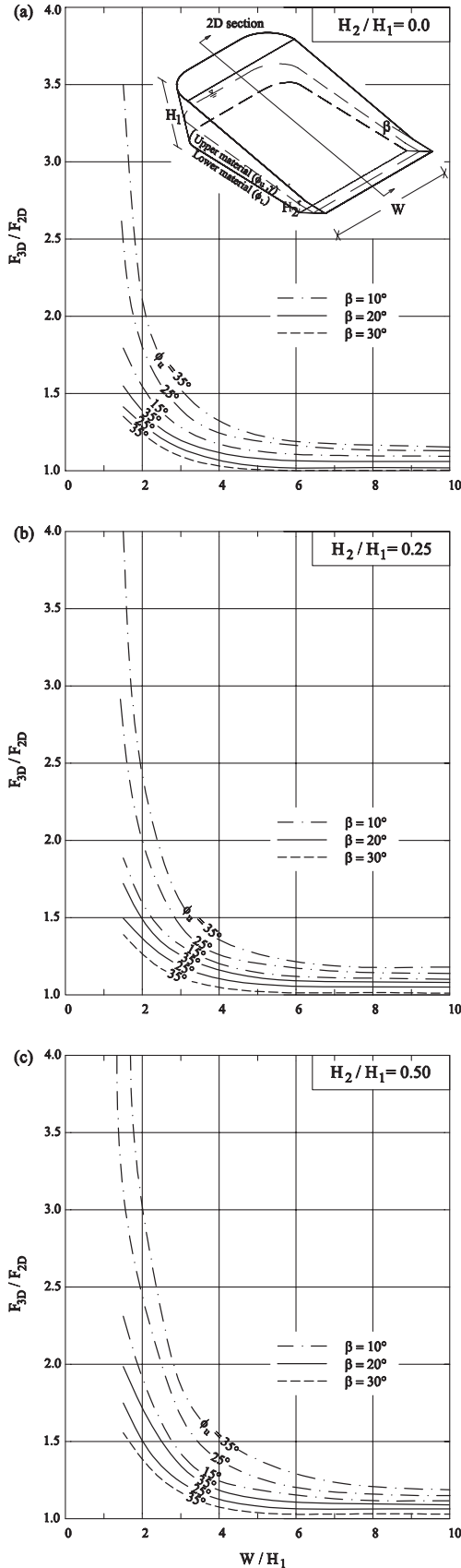
(b) Forces generated by water pressure

$W/H_1$ ,  $\beta$ , and  $\phi_U$  the 3D effect increases with increasing  $H_2/H_1$  value. Increasing  $H_2/H_1$  magnifies the effect of changing  $\beta$  on the calculated  $F_{3D}/F_{2D}$  for slopes with the same  $W/H_1$  and  $\phi_U$ , especially in cases of low values of  $W$ . This is attributed to a greater shear resistance being developed along the vertical sides due to the increase of their areas with increasing  $H_2/H_1$  ratio.

Figure 11 also shows that the value of  $F_{3D}/F_{2D}$  increases with decreasing  $\beta$ . This can be attributed also to the enlargement of the vertical side area, especially at the middle wedge of flatter slopes, which leads to relatively greater shear resistance along the sides and consequently a higher 3D effect. The figure also shows an increase of the 3D effect with increasing value of  $\phi_U$ . This value influences the magnitude of shear resistance along the vertical sides of sliding mass in two opposite ways. Higher  $\phi_U$  leads to a lower value of the at-rest coefficient used in calculating earth pressure forces that are applied perpendicular to the vertical sides. On the other hand, it leads to a higher value of shear strength coefficient ( $\tan \phi_U$ ) by which the earth pressure forces are multiplied to estimate the shear resistance along those sides (Fig. 10). For the slope conditions considered in this study, the resultant of these two contrary influences yields a higher shear resistance and consequently an increase of the 3D effect with increasing  $\phi_U$ . Because of the difference in utilized failure mode and shear strength representation, this type of resultant influence of  $\phi_U$  on the 3D effect is not in agreement with that reported by several researchers (e.g., Chen 1981; Lovell 1984; Duncan 1996; Farzaneh and Askari 2003) of a decrease in the importance of 3D analysis with the increase of the value of friction angle ( $\phi'$ ) for circular or log-spiral slips through homogenous or nonhomogenous soils, the shear strength of which is described using both friction angle and cohesion.

Utilizing the charts shown in Figs. 6b, 7, 8, 9, and 11 leads to a complete definition of the 3D geometrical configuration of potential critical sliding mass if the parameters  $\beta$ ,  $\phi_U$ ,  $\phi_L$ ,  $\gamma$ ,  $\delta$ ,  $H_1$ ,  $H_2$ , and  $H_w$  are known for the critical 2D

**Fig. 11.** The effect of sliding mass geometry and material shear strength on the ratio of  $F_{3D}$  to  $F_{2D}$  for slope models with: (a)  $H_2/H_1 = 0.0$ ; (b)  $H_2/H_1 = 0.25$ ; (c)  $H_2/H_1 = 0.5$ .



section that has  $F_{2D} < 1.0$ . The length of this critical mass can be calculated once the value of  $X$  is determined using Fig. 6b. The value of  $F_{2D}$  is then estimated utilizing one of Figs. 7–9 to be used in determining the width of the critical mass utilizing Fig. 11 by assigning a value of 1.0 to  $F_{3D}$ . This analysis leads to describing a slope failure scenario that starts with having sections where  $F_{2D} < 1.0$ . For failure to occur, the back scarp of a mass including these sections should extend laterally to decrease the end effect relative to the driving forces until a critical mass width is reached and  $F_{3D} = 1.0$  is mobilized. This means that failure through regular slopes should have almost the same sliding mass width that is equal to the critical mass width. This conclusion is supported by width regularity of sliding masses, described for slope failures by several researchers (e.g., Bromhead 1986).

**Pseudostatic seismic effect**

Seismic loads acting on the slope model were considered in the development of the charts shown in Fig. 12 by including a pseudostatic force due to seismic acceleration. Forces were imposed at the center of gravity of the proposed sliding mass. Values of 0.1 and 0.2 were assigned to the coefficient  $K_h$  that represents the intensity of horizontal acceleration as a fraction of gravity acceleration ( $g$ ). For simplicity, the ratio of the 3D factor of safety considering seismic loads ( $F_{3D(seismic)}$ ) to the critical cross-section factor of safety without considering them ( $F_{2D}$  or  $F_{2D(static)}$ ) was used for the charts presented in Fig. 12 to illustrate the combined 3D and seismic effects on the stability of slopes. Comparing the charts of Fig. 12 to those of Fig. 11 shows that in spite of including the effect of side shear resistance, consideration of the seismic forces rendered the  $F_{3D(seismic)}/F_{2D}$  ratio to be lower than 1.0 even for the relatively high values of  $H_2/H_1$ .

Considering the seismic effect led to a calculated ratio for  $F_{3D(seismic)}/F_{2D}$  that is insensitive to the value of  $\phi_U$ . As a result, curves of different  $\phi_U$  for each slope inclination  $\beta$  used in Fig. 11 were combined in Fig. 12 in one curve for that slope due to seismic effect consideration. This means that, for the range of parameters considered in this study, the  $F_{3D(seismic)}/F_{2D}$  value is geometrically related and practically does not depend on material properties. It should be noticed also that  $F_{3D(seismic)}/F_{2D}$  decreases with decreasing  $\beta$  (Fig. 12). This can be attributed to the greater effect of applying seismic forces in reducing the 3D factor of safety in case of lower slope angles. A similar conclusion can be drawn from data presented by Michalowski (2002) for slopes with log-spiral failure surfaces.

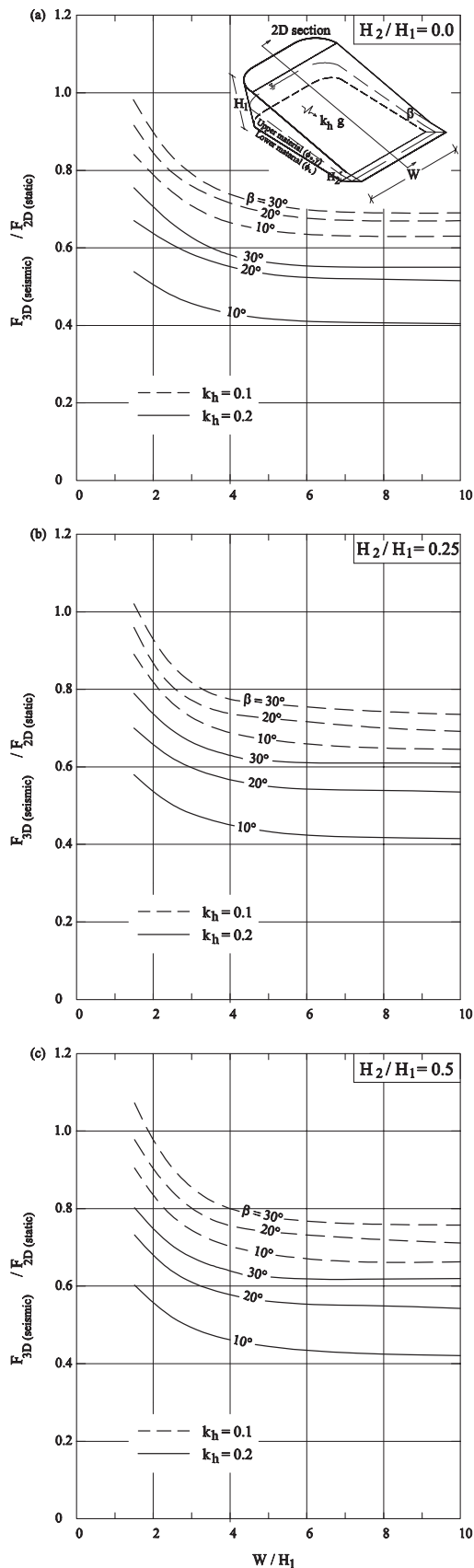
**Numerical examples**

The following four examples illustrate some uses of the 2D and 3D stability charts presented in this paper.

**Example 1**

Let a slope be comprised of soil whose  $\phi' = 30^\circ$  and  $\gamma = 20 \text{ kN/m}^3$  placed on an existing horizontal layer of soil with  $\phi' = 15^\circ$ . Determining the slope inclination ( $\beta$ ) that allows for  $F_{2D} = 1.5$  against translational failure requires the use of the chart in Fig. 7a. Using values of  $\tan \phi_L / \tan \phi_U =$

**Fig. 12.** The effect of sliding mass geometry on the ratio of  $F_{3D(\text{seismic})}$  to  $F_{2D(\text{static})}$  for slope model subjected to pseudostatic horizontal force: (a)  $H_2/H_1 = 0.0$ ; (b)  $H_2/H_1 = 0.25$ ; (c)  $H_2/H_1 = 0.5$ .



$\tan 15^\circ / \tan 30^\circ = 0.464$  and  $F_{2D} / \tan \phi_U = 1.5 / \tan 30^\circ = 2.6$ , we read  $\beta = 25^\circ$ .

**Example 2**

Let a 12 m high slope with a  $20^\circ$  inclination be cut in a 16 m thick layer of homogenous soil with  $\phi' = 35^\circ$  and  $\gamma = 20 \text{ kN/m}^3$  that is underlain by an extended layer of soil with  $\phi' = 10^\circ$  and inclined surface of  $3^\circ$  down slope (i.e.,  $\delta = 3^\circ$ ). Evaluating  $F_{2D}$  that is the same for both  $\phi_U$  and  $\phi_L$  does not require an iterative procedure. Using  $H_2/H_1 = 4/16 = 0.25$  and  $\tan \phi_L / \tan \phi_U = \tan 10^\circ / \tan 35^\circ = 0.252$ , we read in Fig. 8b that  $F_{2D} / \tan \phi_U = 2.36$ . This yields  $F_{2D} = 2.36 \times \tan 35^\circ = 1.65$ .

**Example 3**

A slope failed in translational mode with the following parameters:  $\beta = 10^\circ$ ,  $W/H_1 = 4$ ,  $H_2/H_1 = 0$ ,  $H_W/H_1 = 0.4$ ,  $\phi_U = 25^\circ$ ,  $\gamma = 17 \text{ kN/m}^3$ ,  $\delta = 0$ . Back-calculation of  $\phi_L$  value mobilized at failure requires the use of Figs. 11a and 7d. From Fig. 11a we read  $F_{3D}/F_{2D} = 1.25$ . Since  $F_{3D} = 1.0$  at failure,  $F_{2D} = 1.0/1.25 = 0.8$ . With the given  $\phi_U$ ,  $\beta$ , and  $\gamma$ , we read from Fig. 7d  $\tan \phi_L / \tan \phi_U = 0.16$ , which gives  $\phi_L = 4.3^\circ$ . This means that the required lower soil friction angle mobilized at failure  $(\phi_L)_{\text{mob}} = 4.3^\circ$ . It should be noted that if the 3D effect is not considered in this example, the back-calculated friction angle  $(\phi_L)_{\text{mob}}$  will be overestimated to  $5.8^\circ$ , which is a result of using Fig. 7d with  $F_{2D} = 1.0$ .

**Example 4**

If the slope described in Example 3 has a  $\phi_L$  of  $10^\circ$ , the 3D factor of safety under static and seismic ( $k_h = 0.1$ ) conditions can be calculated using Fig. 7d, which indicates a value for  $F_{2D}$  of 1.43, and then Figs. 11a and 12a, which indicate  $F_{3D}/F_{2D} = 1.25$  and  $F_{3D(\text{seismic})}/F_{2D} = 0.67$ , respectively. This yields  $F_{3D} = 1.25 \times 1.43 = 1.79$ , and  $F_{3D(\text{seismic})} = 0.67 \times 1.43 = 0.96$ .

**Conclusions**

A set of 2D and 3D stability charts was produced for slopes susceptible to translational failure based on an extensive parametric study. The presented charts do not require an iterative procedure in estimating factor of safety. They are also unlike the few available ones dealing with translational failure mode by being more comprehensive concerning the utilized sliding mass configurations, material unit weight and shear strength parameters, pore-water pressure and loading conditions, and method of quantifying and incorporating the 3D end effect, which is especially important for stability analysis of slopes failing in such mode. The following results are concluded and interpreted based on the 2D and 3D slope stability analyses performed in the parametric study.

- (1) The simple wedge method overestimates  $F_{2D}$  against translational failure, while the NAVFAC (1971) wedge method underestimates it. The error magnitude is enhanced for higher values of  $H_2$  and  $\phi_L$  and insensitive to values of  $\beta$  and  $\phi_U$ .
- (2) Using one average value for  $r_u$  overestimates the pore-water pressures and consequently leads to underestimation of  $F_{2D}$ . This error increases with a decrease in  $\phi_L$ . As a result, representing pore-water pressure by intro-

ducing water table elevations is recommended for translational failure analysis of slopes.

- (3) The top width of the critical sliding mass increases with increasing values of  $\beta$  and  $H_2/H_1$  and decreasing values of  $\phi_L$ . It is insensitive to values of  $\delta$  and  $\phi_U$ . The width should be determined before any further stability analysis because it defines the critical slip surface location. A chart was presented for this purpose.
- (4) The value of  $F_{2D}$  depends on the ratio of  $H_2$  to  $H_1$  rather than on their absolute values. It increases with increasing values of  $H_2/H_1$ ,  $\phi_U$ ,  $\phi_L$ , and  $\gamma$ , and decreasing values of  $H_W$ ,  $\beta$ , and  $\delta$ . The effect of flattening the slope to increase the factor of safety decreases in cases of low  $\phi_L$  to  $\phi_U$  ratio. The influence of changing  $\gamma$  on  $F_{2D}$  values decreases with increasing  $\beta$ , and  $\delta$ , and decreasing  $H_W$  values. Unlike the case for rotational failure,  $F_{2D}$  against translational failure decreases with the decrease in the unit weight of the sliding materials that are partly or wholly submerged below the water table. For dry slopes,  $F_{2D}$  is not sensitive to values of  $\gamma$  utilized in this study.
- (5) The value of  $F_{3D}$  is greater than  $F_{2D}$  of the critical cross-section of the same sliding mass regardless of slope geometry configurations and the values of the material properties. For failure to occur, the back scarp of a mass including these sections should extend laterally to decrease the end effect relative to the driving forces until a critical mass width is reached and  $F_{3D} = 1.0$  is mobilized. This means that failure through regular slopes should have almost the same sliding mass width, which is equal to the critical mass width. This conclusion is supported by width regularity of sliding masses described for slope failures by several researchers.
- (6) The 3D effect, i.e.,  $F_{3D}/F_{2D}$  values, increases with decreasing  $W/H_1$  and  $\beta$ , and increasing  $H_2/H_1$  and  $\phi_U$ . The ratio is not sensitive to values of  $\phi_L$ ,  $\delta$ ,  $\gamma$ , and  $H_W$ . Increasing  $F_{3D}$  against translational failure with increasing  $\phi_U$  is not in agreement with reports by several researchers of a decrease in the importance of 3D analysis with an increase in the value of friction angle ( $\phi'$ ) for a circular or log-spiral slip surface through homogenous or nonhomogenous soils, the shear strength of which is described using both friction angle and cohesion.
- (7) The ratio of the 3D factor of safety considering seismic loads ( $F_{3D(\text{seismic})}$ ) to the critical cross section factor of safety without considering them ( $F_{2D}$ ) was used in this study to illustrate the combined 3D and seismic effects on the stability of slopes. For  $k_h$  of 0.1 or 0.2, the seismic effect rendered the  $F_{3D(\text{seismic})}/F_{2D}$  ratio to be lower than 1.0 even with the relatively high values of  $H_2/H_1$ . The  $F_{3D(\text{seismic})}/F_{2D}$  ratio decreases with decreasing  $\beta$  and is not sensitive to values of  $\phi_U$ . As a result, for the range of parameters considered in this study, the value of  $F_{3D(\text{seismic})}/F_{2D}$  is geometrically related and practically does not depend on material properties.

## References

Arellano, D., and Stark, T.D. 2000. Importance of three-dimensional slope stability analysis in practice. *In Proceedings of Slope Stability 2000 Specialty Conference*, Denver, Colo., 5–

- 8 August 2000. American Society of Civil Engineers, Geotechnical Special Technical Publication No. 101, pp. 18–32.
- Baligh, M.M., and Azzouz, A.S. 1975. End effects of stability of cohesive slopes. *Journal of Geotechnical Engineering Division, ASCE*, **101**(11): 1105–1117.
- Barnes, G. 1999. A commentary on the use of the pore pressure ratio  $r_u$  in slope stability analysis. *Ground Engineering*, **32**(8): 38–40.
- Bell, J.M. 1966. Dimensionless parameters for homogenous earth slopes. *Journal of Soil Mechanics and Foundation Engineering Division, ASCE*, **92**(5): 51–65.
- Bishop, A.W. 1955. The use of the slip circle in the stability analysis of slopes. *Géotechnique*, **5**(1): 7–17.
- Bishop, A.W., and Morgenstern, N.R. 1960. Stability coefficient for earth slopes. *Géotechnique*, **10**(4): 129–150.
- Bromhead, E.N. 1986. *The stability of slopes*. Chapman and Hall, N.Y. 373 pp.
- Byrne, R.J., Kendall, J., and Brown, S. 1992. Cause and mechanism of failure, Kettleman Hills Landfill B-19, Unit IA. *In Proceedings of the Specialty Conference on Stability and Performance of Slopes and Embankments-II*, University of California, Berkeley, 29 June – 1 July 1992. American Society of Civil Engineers, Geotechnical Special Technical Publication No. 31. Vol. 2, pp. 1188–1215.
- Chandler, R.J., and Pachakis, M. 1973. Long-term failure of a bank on a solifluction sheet. *In Proceedings of the 8th International Conference on Soil Mechanics and Foundation Engineering*, Moscow. Vol. 2, pp. 45–51.
- Chandler, R.J., Pachakis, M., Mercer, J., and Wrightman, J. 1973. Four long-term failures of embankments founded on areas of landslip. *Quarterly Journal of Engineering Geology*, **6**: 405–422.
- Chen, R.H. 1981. Three-dimensional slope stability analysis. Joint Highway Research Project 81–17, Purdue University, West Lafayette, Ind. 297 pp.
- Chen, R.H., and Chameau, J.L. 1983. Three-dimensional limit equilibrium analysis of slopes. *Géotechnique*, **33**(1): 31–40.
- Cousins, B.F. 1978. Stability charts for simple earth slopes. *Journal of Geotechnical Engineering Division, ASCE*, **104**(2): 267–279.
- Cruden D.M., Thomson, S., and Hoffman, B.A. 1991. Observation of graben geometry in landslides. *In Proceedings of the International Conference on Slope Stability*. Isle of Wight. Thomas Telford Publication, pp. 33–35.
- Duncan, J.M. 1992. State-of-the art: Static stability and deformation analysis. *In Proceedings of the Specialty Conference on Stability and Performance of Slopes and Embankments-II*, University of California, Berkeley, 29 June – 1 July 1992. American Society of Civil Engineers, Geotechnical Special Technical Publication No. 31. Vol. 1, pp. 222–266.
- Duncan, J.M. 1996. State-of-the art: Limit equilibrium and finite-element analysis of slopes. *Journal of Geotechnical Engineering, ASCE*, **122**(7): 577–596.
- Ehlig, P.L. 1992. Evolution, mechanics and mitigation of the Portuguese Bend landslide, Palos Verdes Peninsula, California. *In Engineering Geology Practice in Southern California*. Star Publishing Co., Belmont, Calif., pp. 531–553.
- Eid, H.T. 1996. Drained shear strength of stiff clays for slope stability analyses. Ph.D. thesis, University of Illinois at Urbana-Champaign, Urbana, Ill.
- Eid, H.T., Stark, T.D., Evans, W.D., and Sherry, P. 2000. Municipal waste slope failure I: Waste and foundation soil properties. *Journal of Geotechnical and Geoenvironmental Engineering, ASCE*, **126**(5): 397–407.
- Ellebody, A.M. 1985. Analysis of Mokattam rockfalls. *In Proceedings of the 11th International Conference on Soil Me-*

- chanics and Foundation Engineering, San Francisco. A.A. Balkema, Rotterdam, The Netherlands. Vol. 4, pp. 2321–2324.
- Esu, F. 1966. Short-term stability of slopes in unweathered jointed clays. *Géotechnique*, **16**(4): 321–328.
- Farzaneh, O., and Askari, F. 2003. Three-dimensional analysis of nonhomogenous slopes. *Journal of Geotechnical and Geoenvironmental Engineering*, ASCE, **129**(2): 137–145.
- Gens, A., Hutchinson, J.N., and Cavounidis, S. 1988. Three-dimensional analysis of slides in cohesive soils. *Géotechnique*, **38**(1): 1–23.
- Hungr, O. 1988. CLARA: Slope stability analysis in two or three dimensions. O. Hungr Geotechnical Research, Inc., Vancouver, B.C.
- Hutchinson, J.N. 1967. The free degradation of London clay cliffs. *In Proceedings of the Geotechnical Conference on Shear Strength of Natural Soils and Rocks*. NGI, Oslo. Vol. 1, pp. 113–118.
- Janbu, N., Bjerrum, L., and Kjaernsli, B. 1956. Soil mechanics applied to some engineering problems. Norwegian Geotechnical Institute Publication No. 16, Oslo, Norway. 93 pp. [In Norwegian with English summary.]
- Jaspar, J.L., and Peters, N. 1979. Foundation performance of Gardiner Dam. *Canadian Geotechnical Journal*, **16**: 758–788.
- Kavazanjian, E., Jr., Matasovic, N., Bonaparte, R., and Schmertmann, G.R. 1995. Evaluation of MSW properties for seismic analysis. *In Proceedings of GeoEnvironment 2000 Specialty Conference*, New Orleans, La., 24–26 February 1995. American Society of Civil Engineers, Geotechnical Special Technical Publication No. 46. Vol. 2, pp. 1126–1141.
- Krahn, J., Johnson, R.F., Fredlund, D.G., and Clifton, A.W. 1979. A highway cut failure in Cretaceous sediments at Maymont, Saskatchewan. *Canadian Geotechnical Journal*, **16**: 703–715.
- Lambe, T.W., and Whitman, R.V. 1969. *Soil mechanics*. John Wiley & Sons, Inc., N.Y. 553 pp.
- Leshchinsky, D., and Baker, R. 1986. Three-dimensional slope stability: end effects. *Soils and Foundations*, **26**(4): 98–110.
- Leshchinsky, D., Baker, R., and Silver, M. 1985. Three dimensional analysis of slope stability. *International Journal for Numerical Methods in Geomechanics*, **9**(2): 199–223.
- Lovell, C.W. 1984. Three dimensional analysis of landslides. *In Proceedings of the 4th International Symposium on Landslides*, Toronto, Ont. University of Toronto Press, Toronto. Vol. 2, pp. 451–455.
- Madej, J.S., and Gajewski, K. 1988. On the simplified solution of the three-dimensional slope stability analysis. *In Proceedings of the 5th International Symposium on Landslides*, Lausanne, Switzerland. A.A. Balkema, Rotterdam, The Netherlands. Vol. 1, pp. 719–723.
- Mesri, G., and Abdel-Ghaffar, M.E.M. 1993. Cohesion intercept in effective stress-stability analysis. *Journal of Geotechnical Engineering*, ASCE, **119**(8): 1229–1249.
- Mesri, G., and Cepeda-Diaz, A.F. 1986. Residual shear strength of clays and shales. *Géotechnique*, **36**(2): 269–274.
- McCallum, R.T. 1930. The opening-out of Coften tunnel L.M.S. railway. *In Proceedings of Institute of Civil Engineering*. Vol. 231, Part 1, pp. 161–187.
- Michalowski, R.L. 2002. Stability charts for uniform slopes. *Journal of Geotechnical and Geoenvironmental Engineering*, ASCE, **128**(4): 351–355.
- Montés, P., Silvestri, V., and Soulié, M. 1996. Slope stability analysis and charts for non-circular slip surface. *In Proceedings of the 7th International Symposium on Landslides*, Trondheim, Norway. A.A. Balkema, Rotterdam, The Netherlands. Vol. 2, pp. 1305–1310.
- NAVFAC. 1971. Design manual: Soil mechanics, foundations, and earth structures, NAVFAC, DM-7. US Department of Navy, Naval Facilities Engineering Command, Alexandria, Va.
- O'Connor, M.J., and Mitchell, R.J. 1977. An extension of the Bishop and Morgenstern slope stability charts. *Canadian Geotechnical Journal*, **14**: 144–151.
- Qian, X., Koerner, R.M., and Gray, D.H. 2003. Translational failure analysis of landfills. *Journal of Geotechnical and Geoenvironmental Engineering*, ASCE, **129**(6): 506–519.
- Sauer, E.K., and Christiansen, E.A. 1987. The Denholm landslide, Saskatchewan, Canada, an update. *Canadian Geotechnical Journal*, **24**: 163–168.
- Scranton, H.B. 1996. Field performance of sloping test plots containing geosynthetic clay liners. M.Sc. thesis. University of Texas at Austin, Austin, Tex.
- Seed, R.B., Mitchell, J.K., and Seed, H.B. 1990. Kettleman Hills waste landfill slope failure II: Stability analysis. *Journal of Geotechnical and Engineering*, ASCE, **116**(4): 669–689.
- Singh, A. 1970. Shear strength and stability of man-made slopes. *Journal of Soil Mechanics and Foundation Engineering*, ASCE, **96**(6): 1879–1892.
- Skempton, A.W. 1953. Soil mechanics in relation to geology. *Proceedings of Yorkshire Geological Society*, **29**: 33–62.
- Skempton, A.W. 1985. Residual strength of clays in landslides, folded strata and the laboratory. *Géotechnique*, **35**(1): 3–18.
- Skempton, A.W., and Petley, D.J. 1967. The strength along structural discontinuities in stiff clays. *In Proceedings of the Geotechnical Conference on Shear Strength of Natural Soils and Rocks*. NGI, Oslo, Norway. Vol. 2, pp. 29–46.
- Spencer, E. 1967. A method of analysis of the stability of embankments assuming parallel inter-slice forces. *Géotechnique*, **17**(1): 11–26.
- Stark, T.D., and Eid, H.T. 1992. Comparison of field and laboratory residual shear strengths. *In Proceedings of the Specialty Conference on Stability and Performance of Slopes and Embankments-II*, University of California, Berkeley, 29 June – 1 July 1992. American Society of Civil Engineers, Geotechnical Special Technical Publication No. 31. Vol. 1, pp. 876–889.
- Stark, T.D., and Eid, H.T. 1994. Drained residual strength of cohesive soils. *Journal of Geotechnical Engineering*, ASCE, **120**(5): 856–871.
- Stark, T.D., and Eid, H.T. 1997. Slope stability analyses in stiff fissured clays. *Journal of Geotechnical and Geoenvironmental Engineering*, ASCE, **123**(4): 335–343.
- Stark, T.D., and Eid, H.T. 1998. Performance of three-dimensional slope stability methods in practice. *Journal of Geotechnical and Geoenvironmental Engineering*, ASCE, **124**(11): 1049–1060.
- Stark, T.D., and Poeppel, A.R. 1994. Landfill liner interface strengths from torsional-ring-shear tests. *Journal of Geotechnical Engineering*, ASCE, **120**(3): 597–615.
- Stark, T.D., Eid, H.T., Evans, W.D., and Sherry, P. 2000. Municipal waste slope failure II: Stability analyses. *Journal of Geotechnical and Geoenvironmental Engineering*, ASCE, **126**(5): 408–419.
- Taylor, D.W. 1937. Stability of earth slopes. *Journal of the Boston Society of Civil Engineers*, **24**: 197–246.
- Vargas, M., and Pichler, E. 1957. Residual soil and rock slides in Santos, Brazil. *In Proceedings of the 4th International Conference on Soil Mechanics and Foundation Engineering*, London. Vol. 2, pp. 394–398.
- Wright, S.G. 1992. UTEXAS3: A computer program for slope stability calculations, Geotechnical Engineering Software GS86–1, Department of Civil Engineering, University of Texas, Austin, Tex.